Forward gluon production in hadron–hadron scattering with Pomeron loops

E. Iancu[1], C. Marquet, G. Soyez[2]

Service de Physique Théorique, CEA/DSM/SPhT, Unité de recherche associée au CNRS (URA D2306), CEA Saclay, F-91191 Gif-sur-Yvette, France

Abstract

We discuss new physical phenomena expected in particle production in hadron–hadron collisions at high energy, as a consequence of Pomeron loop effects in the evolution equations for the Color Glass Condensate. We focus on gluon production in asymmetric, 'dilute–dense', collisions : a dilute projectile scatters off a dense hadronic target, whose gluon distribution is highly evolved. This situation is representative for particle production in proton–proton collisions at forward rapidities (say, at LHC) and admits a dipole factorization similar to that of deep inelastic scattering (DIS). We show that at sufficiently large forward rapidities, where the Pomeron loop effects become important in the evolution of the target wavefunction, gluon production is dominated by 'black spots' (saturated gluon configurations) up to very large values of the transverse momentum, well above the *average* saturation momentum in the target. In this regime, the produced gluon spectrum exhibits *diffusive scaling*, so like DIS at sufficiently high energy.

---

[1] Membre du Centre National de la Recherche Scientifique (CNRS), France.
[2] On leave from the Fundamental Theoretical Physics group of the University of Liège.

1 Introduction

The recent data on particle production at semi–hard transverse momenta ($p_\perp = 1 \div 5$ GeV) in deuteron–gold (d+Au) collisions at RHIC [1–3] show strong evidence in favour of high gluon density effects in the nuclear target and can be naturally accommodated [4–14] within the same theoretical framework that has been previously used to describe the HERA data at small Bjorken–x [15] : the effective theory for non–linear evolution in QCD at high energy known as the "Color Glass Condensate" (CGC) [16, 17] (see the review papers [18] for details and more references).

In particular, the results at RHIC show a striking difference between the particle yield at central and, respectively, forward rapidities — namely, a very rapid evolution of the nuclear modification factor R_{dAu} from a 'Cronin peak' ($R_{\mathrm{dAu}} > 1$) at central rapidity ($\eta = 0$) to 'high–$p_\perp$ suppression' ($R_{\mathrm{dAu}} < 1$) at forward rapidity ($\eta > 1$); see, e.g., the discussion in [19] — which is naturally attributed to the small–x evolution of the gluon distribution in the nucleus in the presence of non–linear effects [4, 6, 8, 10, 13]. (One should recall at this point that increasing η is tantamount to probing gluons with smaller values of x in the nuclear wavefunction; see the discussion of kinematics in Sect. 2.) Moreover, for very forward rapidities ($\eta \geq 3$), the spectrum of the produced hadrons appears to be consistent with *geometric scaling* [20], which is a hallmark of the BFKL evolution in the vicinity of the saturation line [21–23]. For smaller rapidities $0 \leq \eta < 3$, the *violations* of this scaling become visible too [14], and they indeed follow the pattern predicted by the CGC effective theory [21–23] — a pattern which has been also verified in the HERA data for the F_2 structure function at $x < 0.01$ [15].

These results at RHIC demonstrate the potential of the 'dilute–dense' (here, deuteron–gold) hadron–hadron collisions to accurately probe the universal phase of QCD at high energy — the Color Glass Condensate. We expect this potential to be amplified in the incoming experiments at LHC, because of the considerably higher energies that will be available there. One should emphasize here that such asymmetric collisions, in which one of the partaking hadrons (the 'projectile') is dilute and the other one (the 'target') is dense, are exceptional in several respects:

• On the *experimental* side, the 'dilute–dense' collisions are less affected by the final–state interactions than the 'dense–dense' collisions (like the nucleus–nucleus ones), hence they represent a relatively clean measurement of the initial conditions (nearly on the same footing as the deep inelastic lepton–hadron scattering).

• On the side of the *theory*, such collisions are better under control, in the sense that factorization schemes are available, which allow one to compute the cross–section for particle production as a convolution of (standard) parton distributions for the dilute projectile times 'generalized parton distributions' (including high–density effects) for the dense target times partonic cross–sections [9, 24–29]. This factorization is very similar to the 'dipole factorization' used for DIS at high energy (see, e.g., Ref. [18] and references therein), and the 'generalized parton distributions' alluded to above are in fact *dipole–hadron scattering amplitudes* [30], which describe the multiple scattering between a 'color dipole' and the dense hadronic target.

Hence, the non–trivial scattering problem that one has to solve is that of the scattering between an elementary color dipole and the high–density hadronic target. To that aim, one can rely on the CGC formalism [18], where the dipole amplitudes obey an infinite hierarchy of non–linear evolution equations — the Balitsky–JIMWLK hierarchy [17, 31–33]. In the limit where the number of colors N_c is large, this hierarchy boils down to a single equation, the Balitsky–Kovchegov (BK) equation [31, 34]. Most of the previous analyses of the d+Au collisions within the framework of CGC were based on the solution to BK equation, or on various approximations to it [4, 6, 8, 10]; as mentioned before, they led to a rather satisfactory picture, which provides a qualitative explanation [3] of the experimental situation at RHIC and is robust against the various approximations.

But whereas the current CGC formalism, centered around the JIMWLK equation and its main consequences like 'geometric scaling', appears to be appropriate for understanding the experimental situation at RHIC and HERA, it is not clear whether this success will extend to the future data at LHC. Indeed, recent theoretical developments [35–45] show that some physical ingredients which have been ignored by the JIMWLK evolution play an increasingly important role with increasing energy, and should lead to a dramatically different physical picture at sufficiently high energy. These ingredients are the *gluon–number fluctuations* [35, 37, 46, 47] associated with gluon splitting (bremsstrahlung) in the dilute regime, which act as a seed for κ–body correlations with $\kappa \geq 2$. Although formally suppressed by higher powers of the coupling constant α_s, such correlations are rapidly amplified by the BFKL evolution (the faster the larger is κ) and eventually play an essential role in the evolution towards gluon saturation at high energy. The Balitsky–JIMWLK equations correctly encode the role of such many–body correlations in providing saturation, but they fail to include the physical *source* for such correlations, namely, the gluon–number fluctuations at low density [38]. Thus, while these equations are properly describing the evolution of a dense system towards saturation, they cannot describe the formation of such a dense system via evolution from a dilute system at low energy.

At this point, one may be tempted to conclude that the Balitsky–JIMWLK equations should at least apply to the evolution of a large nucleus, which starts with a relatively high gluon density already at low energy. However, this is not true either ! Even for a large nucleus, the gluon distribution involves a dilute tail at relatively high transverse momenta (well above the nuclear saturation momentum), and the evolution of that tail is still dominated by fluctuations. It is nevertheless true that, in order to probe the effects of fluctuations for such a large nucleus, one needs to go up to much higher energies, namely, high enough for the saturation effects to have propagated at relatively large transverse momenta, which were originally in the dilute tail at low energy. In that sense, the evolution of a *originally dilute* system, like a proton or a color dipole, is a better laboratory to study the effects of fluctuations.

The equations describing gluon evolution in the presence of both saturation and fluctuations are presently known only for large N_c, and are generally referred to as the

---

[3] Quantitative fits have been also obtained [11, 13, 14], but only at the expense of introducing some free parameters, to account for the lack of accuracy of the current formalism and for the uncertainties associated with the non–perturbative initial conditions. It is interesting to note that most of these parameters were in fact fixed from fits to the HERA data for F_2.

'Pomeron loop equations' [38–40, 42]. The 'Pomeron' here is the BFKL Pomeron [48]; namely, this is the amplitude for the scattering between an external dipole and the target in the linear, leading–logarithmic, approximation at high energy. In an appropriate gauge, this amplitude has a diagrammatic interpretation in terms of ladder diagrams whose rungs are strongly ordered in the 'rapidity' variable $Y \equiv \ln(1/x)$. At large N_c, the gluon bremsstrahlung (responsible for gluon number fluctuations) can be described as $1 \to 2$ Pomeron splitting, while the saturation effects are tantamount to $2 \to 1$ Pomeron merging. Hence, the equations describing the complete evolution involve both (Pomeron) splitting and merging, and thus generate Pomeron loops through iterations.

The Pomeron loop equations form an infinite hierarchy, with a complicated non–local structure, and in spite of intense theoretical efforts, their general solutions are not yet known. Still, the asymptotic behaviour of the solutions at high energy is known because of the *universality of the stochastic process described by these equations* [37, 49–51] : this is in the same universality class as the 'reaction–diffusion' process $A \rightleftharpoons 2A$, which is relevant to a large variety of problems (in statistical physics, chemistry, biology ...) and has been intensely scrutinized over the last decades (cite Ref. [52] for a review). But even in that context, it was only recently realized that this process is extremely sensitive to particle–number fluctuations in the dilute regime [53]. In the language of QCD, this sensitivity explains why the predictions of the Pomeron loops equations turn out to be very different from those of the Balitsky–JIMWLK equations, which ignore fluctuations [36–38].

By using known results from statistical physics [52, 53], it has been possible to deduce the functional form of the dipole scattering amplitudes in QCD at high energy and large N_c, in terms of juste a couple of uncontrolled parameters [38]. The most striking feature of these results is the fact that, even in the *weak scattering* regime, that is, for a relatively small projectile dipole, the scattering amplitude is dominated by *black spots*, i.e., rare gluon configurations which are at saturation on the resolution scale $Q^2 \sim 1/r^2$ of the projectile (r is the dipole size) and thus look 'black' to the latter — the dipole is completely absorbed when hitting any such a spot. The reason why the *average* amplitude is nevertheless small is because such 'black spots' are relatively rare, so the target disk looks transparent (or 'white') on that resolution scale at most impact parameters (see Sect. 3 for details).

Very recently, the consequences of this new physical picture have been explicitly worked out for the case of DIS [45], with the conclusion that new phenomena are to be expected at very high energy — chiefly among them, the replacement of geometric scaling by a new, *diffusive*, scaling which should extend up to very large Q^2 (cf. Sect. 3). But whereas in the case of DIS, it is not clear when, and whether, new experiments will become available with sufficiently high energy to probe this new physics (as aforementioned, the current experimental situation at HERA is consistent with geometric scaling, thus suggesting an *intermediate–energy* regime), the imminent advent of the LHC opens the possibility to observe the Pomeron loops via high–energy hadron–hadron collisions.

Both pp and pA (and also AA) collisions will be performed at LHC, but for the reasons explained earlier, the best process to study the fluctuation–dominated regime at high energy is particle production at forward rapidities in pp collisions. Then, one of the participating protons (the 'projectile') is dilute and acts as a probe of the small–x part of the wavefunction of the other proton (the 'target'), which is highly evolved. Ideally,

one needs very large forward rapidities for the produced particles, in order to generate a large asymmetry between the evolutions of the target and the projectile, and thus probe Pomeron loop effects in the target proton while keeping the projectile proton dilute.

In view of the theoretical uncertainties alluded to above, it is not possible for us today to make quantitative predictions for LHC, and not even to reliably predict whether the new physics should manifest itself within the kinematical range covered by the LHC, or not. What we *can* do, however, is to predict new, qualitative, phenomena which would unambiguously signal the new physics in the data for particle production, and even compute these phenomena in terms of few free parameters. By comparing these predictions to the data to become later available at LHC, one should be able to identify this new physics (if it is present indeed !) and extract the values of the relevant parameters.

Our main purpose here is to demonstrate the consequences of the Pomeron loop physics on the particle production in hadron–hadron collisions at high energy. To that aim, we shall focus on a problem which is conceptually transparent and avoids unnecessary complications[4] : that of the forward gluon production in onium—hadron scattering at high energy and large N_c.

● The *'onium'* is a dilute hadronic system produced via the BFKL evolution of a small color dipole. Its wavefunction is explicitly known within perturbative QCD at large N_c [46], and this is why we have chosen it as a projectile. But the generalization of our subsequent results to a more realistic projectile, like a (dilute) proton, is straightforward: In the most interesting kinematical region, the projectile is merely represented by the standard (integrated) gluon distribution function, as determined by the leading–twist, DGLAP, approximation.

● The *hadronic target* will be assumed to be probed at very small values of x (corresponding to very forward rapidities for the produced gluon), in the fluctuation–dominated regime which is *universal* : this is the ultimate form of hadronic matter which is produced at sufficiently high energy starting with arbitrary initial conditions at low energy. In this regime, the dipole–target scattering amplitude can be taken in the simplified functional form predicted by the correspondence with statistical physics, which represents an approximate solution to the Pomeron loop equations. This functional form describes not only the diffusive scaling regime at asymptotically high energies, but also the geometric scaling regime at intermediate energies, and the transition between the two. Hence, by increasing the rapidity of the produced gluon, we shall be able to study the increasing influence of fluctuations on the cross–section for particle production and the interplay between geometric and diffusive scaling.

This paper is organized as follows: The first two sections contain no new results, but rather collect some previous results — concerning the dipole factorization of forward gluon production (in Sect. 2) and, respectively, the calculation of the dipole amplitudes in the presence of Pomeron loop (in Sect. 3) — which are necessary for the subsequent analysis. The first issue (the factorization of the gluon production) is rather well established in

---

[4] Like the use of realistic parton distributions or fragmentation functions; note, however, that such 'complications' may become essential and unavoidable in view of realistic applications to the phenomenology.

the literature and will be only succinctly described here. But the second one (the high–energy evolution with Pomeron loops) has met with important developments over the last two years, whose results are perhaps less well known (since spread over several, more technical, papers [36–38, 45]), yet they are essential for our present analysis. To cope with that, in Sect. 3 we shall try to give a self–contained and pedagogical discussion of these recent results. Then, in Sects. 4 and 5, we shall apply them to the analysis of forward gluon production at high energy. We shall separately discuss the relevant 'generalized gluon distribution' (a special Fourier transform of the dipole amplitude) (in Sect. 4) and the cross–section for gluon production (in Sect. 5). We shall point out some interesting differences with respect to the corresponding analysis of DIS in Ref. [45]. But in spite of these differences, the final conclusions are qualitatively similar: the cross–section for forward gluon production is dominated by 'black spots' up to very large values of the gluon transverse momentum and the ensuing spectrum shows diffusive scaling. We shall conclude, in Sect. 6, with a short summary and a list of open problems.

2 Gluon production in onium–hadron scattering: Factorization

In this section, we shall more precisely describe the calculation that we intend to perform and recall the factorization scheme which lies at the basis of this calculation.

As explained in the Introduction, we are interested in gluon production in the asymmetric collision between a *dilute projectile*, whose wavefunction has been evolved in rapidity up to y_1, and a *dense target*, with rapidity $y_2 = Y - y_1 \gg y_1$. (Y is the total rapidity gap between the projectile and the target.) Here, by "dilute" and "dense" we understand that, on the resolution scale set by the transverse momentum $k_\perp$ of the produced particle, the gluon distribution in the projectile can be described in the leading–twist approximation (i.e., its evolution up to y_1 lies within the realm of the linear, DGLAP or BFKL, evolution equations of QCD), whereas the gluon distribution in the target is rather the site of important non–linear phenomena, and is strongly influenced by both saturation and gluon–number fluctuations — hence, by Pomeron loops.

For definiteness, and also for more similarity with the physically interesting case of pp collisions at LHC, we shall consider that the collision is viewed in the center–of–mass frame, and that the two partaking hadrons are identical in that frame — or, more precisely, the *look* identical when probed via particle production at *central* pseudo–rapidity [5], $\eta = 0$. However, differences between the target and the projectile will appear when one considers particle production at *forward* (pseudo)rapidity $\eta > 0$, since in that case one probes rather different gluon evolutions in the respective wavefunctions. Specifically, a gluon emerging with rapidity η and transverse momentum $k_\perp$ has been produced via the fusion of a projectile gluon having longitudinal momentum fraction $x_1 = (k_\perp/\sqrt{s})e^\eta$ with a target gluon for which $x_2 = (k_\perp/\sqrt{s})e^{-\eta}$. We deduce that $y_1 \equiv \ln(1/x_1) = Y/2 - \eta$ and similarly

---

[5] The pseudo–rapidity is defined as $\eta = -\ln\tan(\theta/2)$, with θ the angle between the direction of the produced particle and the collision axis. Our conventions are such that 'forward rapidities', i.e., positive values for η, correspond to particles emitted in the fragmentation region of the projectile. For a produced gluon, the pseudo–rapidity coincides with the standard rapidity.
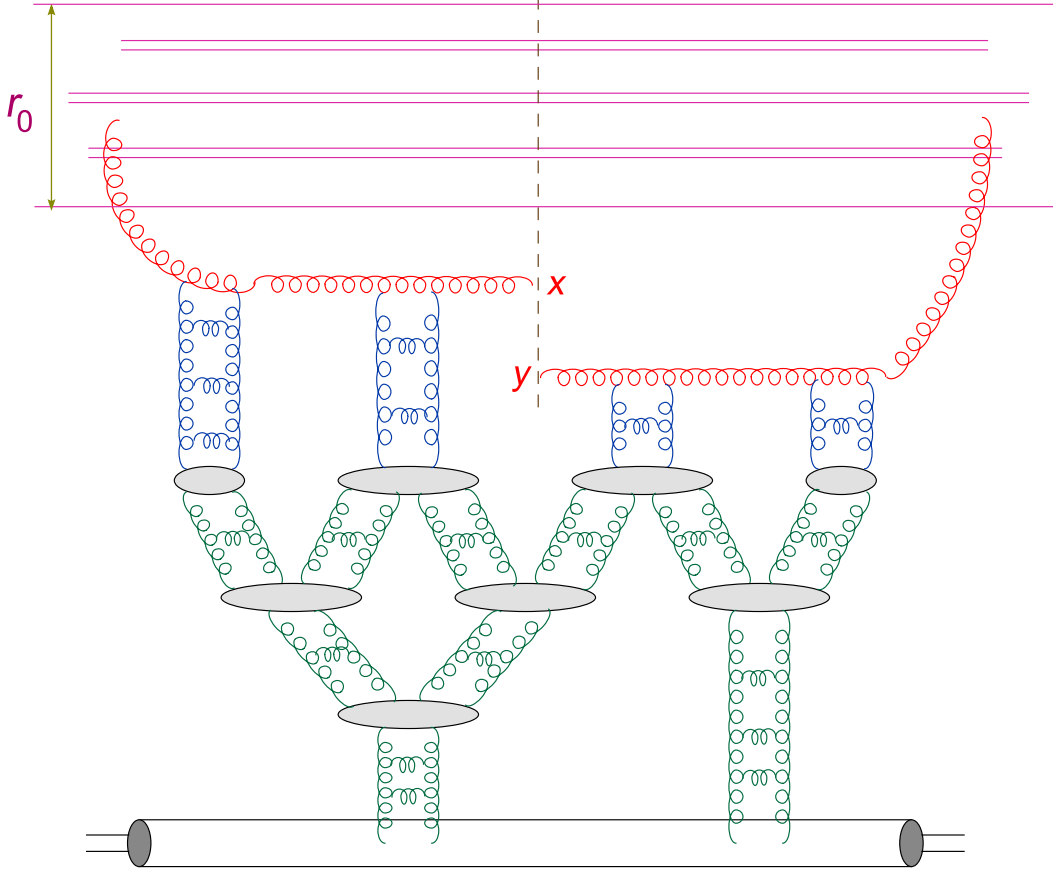
Fig. 1. *A schematic illustration of a Feynman graph contributing to the cross–section for gluon production in onium–hadron scattering in the presence of Pomeron loops. The upper part of the graph represents the 'onium', i.e., the modulus squared of the wavefunction of the BFKL–evolved dipole. Each double–line denotes a soft gluon inside the wavefunction (the gluon is represented as a pointlike quark–antiquark pair in a color octet state, as appropriate at large N_c). The produced gluon (in red) is radiated by one of the dipoles, at transverse coordinate $\boldsymbol{x}$ in the direct amplitude and, respectively, at $\boldsymbol{y}$, in the complex conjugate amplitude. This effectively builds up a gluon–gluon dipole of size $\boldsymbol{r} = \boldsymbol{x} - \boldsymbol{y}$, which multiply scatters off the strong color fields in the target (represented in the lower part of the figure). The evolution of the target wavefunction included Pomeron merging and splitting, hence Pomeron loops.*

$y_2 \equiv \ln(1/x_2) = Y/2 + \eta$, with $Y = \ln(s/k_\perp^2)$. Thus, when both $Y/2$ and η are large enough, but not very different from each other, one can reach the interesting situation where the projectile looks dilute, while the target is dense. More precisely, we shall work under the assumptions that

$$Y,\, \eta \gg \frac{1}{\bar{\alpha}_s} \qquad \text{but} \qquad \frac{Y}{2} - \eta \ll \frac{1}{\bar{\alpha}_s} \ln \frac{1}{\alpha_s^2}\,, \tag{2.1}$$

($\bar{\alpha}_s \equiv \alpha_s N_c/\pi$) where the last condition [35, 46] ensures that saturation effects remain negligible in the (relevant part of the) projectile wavefunction. In fact, the most interesting regime for us here is the high–energy regime at $\bar{\alpha}_s Y > \ln(1/\alpha_s^2)$ (and similarly for $\bar{\alpha}_s \eta$), in which the target wavefunction is sufficiently evolved to be sensitive to Pomeron loops.

Although there is no real need to further specify our target and projectile — since, in the interesting regime at high energy, the cross–section for gluon production is given by a rather universal formula (see Sect. 5) — it is still useful to have a more specific physical picture at hand, at least at intermediate stages. To that aim, we shall assume that the incoming hadronic systems have been produced via the high–energy evolution of an initial quark–antiquark $(q\bar{q})$ dipole of size r_0 (within the large–N_c approximation). Then, the wavefunction of the projectile at rapidity y_1 can be described as an *onium* [46], i.e., a collection of $q\bar{q}$ dipoles which has been generated in the course of the evolution via $1 \to 2$ dipole splitting. On the other hand, the target wavefunction at rapidity y_2 develops saturation effects, so its description transcends the dipole picture, even at large N_c.

Gluon production in onium–hadron scattering can then be described as follows (see also Fig. 1) : a gluon radiated by any of the dipoles within the onium undergoes multiple scattering off the strong color fields in the hadron before eventually emerging with rapidity η and transverse momentum $k_\perp \equiv k$. The differential cross–section for gluon production (or 'gluon spectrum') can be given a factorized structure [9, 24–29, 54]:

$$\frac{\mathrm{d}\sigma}{\mathrm{d}\eta\mathrm{d}^2k\mathrm{d}^2b} = \frac{2\alpha_s C_F}{\pi k^2} \int \frac{\mathrm{d}^2 r_1}{2\pi r_1^2} \, n(r_0, r_1, y_1)$$
$$\int_0^{r_1} \mathrm{d}r \, J_0(kr) \, \log\left(\frac{r_1}{r}\right) \frac{\partial}{\partial r}\left(r \frac{\partial}{\partial r} \, \langle T_{gg}(r)\rangle_{y_2}\right) \tag{2.2}$$

which can be heuristically understood with reference to Fig. 1. The dimensionless quantity $n(r_0, r_1, y_1)$ refers to the onium wavefunction: it represents the density of dipoles of size r_1 produced from the original dipole r_0 after a BFKL evolution up to rapidity $y_1 = Y/2 - \eta$, with the initial condition $n(r_0, r_1, 0) = r_0\delta(r_1 - r_0)$. Furthermore, $\alpha_s C_F \ln(r_1/r)$ can be roughly interpreted as the probability that an elementary dipole of size r_1 radiate a gluon–gluon (gg) dipole of size r, the dipole being effectively constructed with a gluon line in the direct amplitude times another one in the complex conjugate amplitude (r is the transverse distance between these two lines). $\langle T_{gg}(r)\rangle_{y_2}$ is the (average) scattering amplitude for the collision between the gg dipole and the hadronic target evolved up to rapidity $y_2 = Y/2 + \eta$. Finally, the Bessel function $J_0(kr)$ together with the integral over r implements the Fourier transform from the dipole size r to the transverse momentum k of the produced gluon. The presence of the derivatives w.r.t. r in Eq. (2.2), for which we have not given any interpretation, makes it clear that our above 'physical interpretation' is rather crude. A better understanding of Eq. (2.2) would require a careful inspection of its derivation in the literature, but this goes beyond our purposes here.

Eq. (2.2) is often referred to as expressing "$k_\perp$–factorization", and it is instructive to understand why. To that aim, it is convenient to first solve the BFKL equation for $n(r_0, r_1, y_1)$ and then insert the result into Eq. (2.2). One thus finds

$$\frac{\mathrm{d}\sigma}{\mathrm{d}\eta\mathrm{d}^2k\mathrm{d}^2b} = \frac{\bar{\alpha}_s}{k^2} \int_0^\infty \mathrm{d}r \, J_0(kr) \, \tilde{n}(r_0, r, y_1) \frac{\partial}{\partial r}\left(r \frac{\partial}{\partial r} \, \langle T_{gg}(r)\rangle_{y_2}\right) \tag{2.3}$$

(we have used $2C_F \approx N_c$ at large N_c together with $\bar{\alpha}_s \equiv \alpha_s N_c/\pi$), where

$$\tilde{n}(r_0, r, y) \equiv \int_C \frac{d\gamma}{2\pi i} \left(\frac{r_0}{r}\right)^{2\gamma} \frac{1}{2\gamma^2} \exp\left(\bar{\alpha}_s y \chi(\gamma)\right), \tag{2.4}$$

is essentially the Mellin representation of the BFKL solution. ($\chi(\gamma)$ is the standard BFKL characteristic function [48] and the contour C in the complex γ plane is chosen as $C = \{\gamma = \gamma_1 + i\gamma_2 \, ; -\infty < \gamma_2 < \infty\}$, with a fixed γ_1 in the range $0 < \gamma_1 < 1$.) Eq. (2.3) is finally rewritten in a form on which $k_\perp$–factorization becomes manifest :

$$\frac{d\sigma}{d\eta d^2 k d^2 b} = \frac{\bar{\alpha}_s}{k^2} \int \frac{d^2 p}{(2\pi)^2} \, \varphi(p, y_1) \Phi(k - p, y_2), \tag{2.5}$$

where

$$\varphi(p, y) \equiv \int \frac{d^2 r}{2\pi} \, e^{ip \cdot r} \, \tilde{n}(r_0, r, y) \tag{2.6}$$

represents (up to a normalization factor of order α_s) the unintegrated gluon distribution in the onium, whereas the quantity

$$\Phi(k, y) \equiv \int d^2 r \, e^{ik \cdot r} \, \nabla_r^2 \, \langle T_{gg}(r) \rangle_y \tag{2.7}$$

can be similarly interpreted as a *generalized* 'unintegrated gluon distribution' for the target, which is however sensitive to the non–linear effects in the target (related to gluon saturation) via the multiple scattering encoded in the dipole amplitude. It is only for sufficiently large k — much larger than the target saturation momentum — that the quantity $(1/\alpha_s)\Phi(k, y)$ reduces (up to a numerical factor) to the standard, leading–twist, unintegrated gluon distribution. Note also that the two distributions defined in Eqs. (2.6) and (2.7) have different dimensions: this is so since, whereas the onium distribution $\varphi(p, y)$ has been already integrated over the transverse area of the onium (so this is 'unintegrated' only with respect to p), the target distribution $\Phi(k, y)$ on the other hand is rather understood at a fixed impact parameter b within the area covered by the target (hence, this is more properly a *gluon occupation factor* in the transverse phase–space).

In previous applications of Eqs. (2.2)–(2.7), one has always treated the wavefunction of the dense hadronic target in the *mean field approximation*, that is, one has included the effects of saturation and multiple scattering — e.g., by computing the dipole scattering amplitude $\langle T_{gg}(r) \rangle_y$ with the Glauber–Mueller formula, or by solving the BK equation — but one has ignored the gluon–number fluctuations (although the applicability of the factorization (2.2) in the presence of Pomeron loops has been noticed[6] by Kovchegov [54]). Our purpose in what follows is to go beyond such previous analyses, by including the effects of the Pomeron loops in the calculation of $\langle T_{gg}(r) \rangle_y$. As we shall see, these effects lead to a dramatically new physical picture at sufficiently high energy.

---

[6] Note, however, that the analysis in Ref. [54] includes only the 'large' Pomeron loops which appear when the collision between the gg dipole and the target is viewed as onium–onium scattering in the center–of–mass (COM) frame — here, the COM of the subsystem made by the gg dipole and the target. Thus, this analysis is limited to not too high energies [35, 46], unlike our present approach where the Pomeron loops are included directly in the target wavefunction.

The Pomeron loop equations are written for dipoles made with quark–antiquark pairs (rather than gluons), but this is not a problem since at high energy the scattering amplitudes for the two types of dipoles (gg and $q\bar{q}$) are simply related to each other. Namely, if S_{gg} and $S_{q\bar{q}}$ denote the respective S–matrices, with $T = 1 - S$, then in the eikonal approximation we have:

$$S_{gg}(r) = \frac{N_c^2}{N_c^2 - 1} S_{q\bar{q}}^2(r) \approx S_{q\bar{q}}^2(r), \tag{2.8}$$

where the last, approximate, equality holds at large N_c, and we have also assumed that the S–matrix is real, as appropriate at high energy; this in turn implies:

$$T_{gg}(r) \equiv 1 - S_{gg}(r) \approx 2T_{q\bar{q}}(r) - T_{q\bar{q}}^2(r). \tag{2.9}$$

Notice that, in the previous formulæ, we have never indicated the dependence of the dipole amplitude upon the dipole impact parameter, but only upon its size. This is for consistency with our subsequent approximations, in which we shall systematically neglect the b–dependence, i.e., we shall compute amplitudes or cross–sections at fixed impact parameter and assume the high–energy evolution to be quasi–local in b.

In the next section we shall concentrate ourselves on the $q\bar{q}$ amplitude $T_{q\bar{q}}(r)$ — that we shall denote simply as $T(r)$ from now on — and recall some recent results concerning the calculation of this amplitude from the Pomeron loop equations. The consequences of these results for the generalized gluon distribution (2.7) and for the cross–section (2.2) for gluon production will be then examined in the subsequent sections.

3   The dipole amplitude: Black spots & Diffusive scaling

If there was not for (gluon–number) fluctuations, i.e., in the mean field approximation to the non–linear evolution in QCD at high energy, the dipole amplitude $T(r, Y)$ at large N_c would be given by the solution to the BK equation [31, 34] — a non–linear generalization of the BFKL equation which is consistent with unitarity. Even in the presence of fluctuations, the BK amplitude remains a reasonable approximation for the *event–by–event* amplitude, and also for the *average* amplitude $\langle T(r) \rangle_Y$ at *intermediate* values of Y. It is therefore useful to begin our discussion with a brief reminder of the BK solution.

I) Although the latter is not known *exactly*, its basic properties are well understood — thanks to a multitude of analytic and numerical studies [8, 21, 22, 49, 55–59] — and a piecewise analytic approximation to it can be written down. To that purpose, it is preferable to measure the dipole size in logarithmic units, by writing:

$$T(r, Y) \equiv T(\rho, Y) \qquad \text{with} \qquad \rho \equiv \ln \frac{r_0^2}{r^2}, \tag{3.1}$$

where r_0 is the unitarization scale in the target at low energy (e.g., if the target starts as a bare dipole at $Y = 0$, then r_0 is the size of that dipole). Note that large values of ρ correspond to small dipole sizes, or to large transverse momenta ($\rho \sim \ln k^2$) after a Fourier transform.

When viewed as a function of ρ for a fixed (and sufficiently large) Y, the BK solution $T(\rho, Y)$ appears as a *front* which interpolates between the unitarity (or 'black disk') limit, $T = 1$, at relatively small values of ρ and 'color transparency', $T \sim e^{-\rho}$, at very large values of ρ, with the transition between the two regimes ('the front region') governed by the BFKL dynamics with saturation boundary conditions (see Eq. (3.2) below). The *position* of the front, conventionally defined as the value $\rho_s(Y)$ at which $T = 1/2$, represents the unitarization scale at rapidity Y, i.e., the *saturation momentum* $Q_s(Y)$ [16, 60] in logarithmic units. Studies of the BK equation [49] or, simpler, of the BFKL equation supplemented with a saturation boundary condition [21, 22], which reads :

$$T(\rho, Y) = 1/2 \qquad \text{for} \qquad \rho = \rho_s(Y) \equiv \ln\left(r_0^2 Q_s^2(Y)\right), \qquad (3.2)$$

reveal that, for large Y, the front propagates at constant speed: $\rho_s(Y) = \lambda_0 \bar{\alpha}_s Y$, with $\lambda_0 \approx 4.88$. Equivalently, the saturation momentum $Q_s(Y)$ rises exponentially with Y [60], with a 'saturation exponent' $\lambda_0 \bar{\alpha}_s$.

The most interesting region for us here is the front region at (roughly) $\rho_s(Y) < \rho < 2\rho_s(Y)$, where the scattering is weak ($T \ll 1$), yet it is significantly influenced by saturation, via the boundary condition (3.2). Within this region, the BK amplitude shows approximate *geometric scaling*, i.e., it depends upon the two kinematical variables ρ and Y only via the difference $z \equiv \rho - \rho_s(Y) = \ln[1/r^2 Q_s^2(Y)]$. More precisely, one finds [21, 22]

$$T(z, Y) \sim z\, e^{-\gamma_0 z} \exp\left\{-\frac{z^2}{2\beta_0 \bar{\alpha}_s Y}\right\} \qquad \text{for} \qquad 1 \ll z \equiv \rho - \rho_s(Y) \ll \rho_s(Y). \quad (3.3)$$

This expression involves the 'anomalous dimension' $\gamma_0 \approx 0.63$ and the BFKL 'diffusion coefficient' $\beta_0 \equiv \chi''(\gamma_0) \approx 48.52$, which are both hallmarks of the BFKL dynamics in the presence of saturation. Note that the last factor in Eq. (3.3), describing *BFKL diffusion*, depends separately upon z and Y, hence it violates geometric scaling. Still, when increasing Y, there is an increasing domain in z — the *geometric scaling window* at $1 \lesssim z \lesssim z_g(Y)$, with $z_g(Y) \sim (2\beta_0 \bar{\alpha}_s Y)^{1/2}$ — within which BFKL diffusion can be neglected, and the BK amplitude shows good geometric scaling: $T \sim z\, e^{-\gamma_0 z}$. On the other hand, for much larger value of $z \gtrsim \rho_s(Y)$, one enters the regime of color transparency, where the BK solution reduces to the standard 'double–logarithmic approximation'. This is the cross–over domain towards the DGLAP dynamics and collinear factorization.

One should stress at this point that all these remarkable predictions of the BK equation — the exponential growth of the saturation momentum with Y, the existence of a window for geometric scaling at moderately high $Q^2 \gg Q_s^2(Y)$, and the violation of this scaling at even higher values of Q^2 — appear to be necessary in order to explain the HERA data at small–x, and the RHIC data for particle production in d+Au collisions at forward rapidities (cf. the discussion in the Introduction). Remarkably, these properties of the mean field approximation are qualitatively preserved after including the NLO corrections to the BFKL equation, but they suffer quantitative modifications [23], which have the right trend to achieve a better description of the data [15].

II) The basic properties of the BK solution are also preserved by fluctuations, but only at the level of the *event–by–event* amplitude, by which we mean the amplitude obtained

after a single realization of the stochastic evolution. Namely, this amplitude can be given the following piecewise approximation [37]

$$
T(z) = \begin{cases} 1 & \text{for } z < 0 \\ e^{-\gamma_0 z} & \text{for } 1 < z < L \\ e^{-z} & \text{for } z \gg L. \end{cases} \tag{3.4}
$$

where $z \equiv \rho - \rho_s(Y)$ denotes the geometric scaling variable, as before, and we have kept only the dominant, exponential, behaviour in each region. As compared to the BK amplitude discussed previously, there are two important differences though:

a) The front velocity λ, which implicitly enters Eq. (3.4) via $\rho_s \equiv \lambda \bar{\alpha}_s Y$, is considerably smaller than the corresponding prediction of the BK equation, $\lambda_0 \approx 4.88$. The difference $\lambda_0 - \lambda$ is analytically under control only in the (physically unrealistic) weak coupling limit [36, 37, 53]. On then obtains

$$
\lambda \simeq \lambda_0 - \frac{\mathcal{C}}{\ln^2(1/\alpha_s^2)} \qquad \text{when} \qquad \alpha_s^2 \to 0 , \tag{3.5}
$$

where the coefficient $\mathcal{C}$ turns out to be quite huge: $\mathcal{C} = \pi^2 \gamma_0 \chi''(\gamma_0) \approx 150$. Note that, when $\alpha_s^2 \to 0$, λ converges towards λ_0 (from the below), but *only very slowly* (logarithmically). The tendency of λ to decrease when increasing α_s^2 is also confirmed by a study of the 'strong noise limit', which shows that in that limit λ vanishes as a power of $1/\alpha_s^2$ [61].

b) The front region, within which the amplitude (3.4) exhibits geometric scaling with the BFKL 'anomalous dimension' $\gamma_0 \approx 0.63$, is *compact*, i.e., it has a finite width L which is independent of Y. Specifically, L is the distance $\rho - \rho_s$ over which the amplitude falls off from its saturation value $T = 1$ to a value of order α_s^2, where the fluctuations wash out completely any mean field behaviour. This condition immediately yields:

$$
L \simeq \frac{1}{\gamma_0} \ln \frac{1}{\alpha_s^2} + O(1) . \tag{3.6}
$$

More precisely, in the early stages of the evolution, the width of the geometric scaling window increases via BFKL diffusion (cf. Eq. (3.3)), until it gets stuck at its maximal value, equal to L. The condition $z_g(Y_{\text{form}}) = L$ determines the front formation rapidity as

$$
\bar{\alpha}_s Y_{\text{form}} \sim \frac{\ln^2(1/\alpha_s^2)}{2\beta_0 \gamma_0^2} . \tag{3.7}
$$

III) But the most spectacular effects of fluctuations appear in the calculation of *expectation values*, so like the *average* amplitude $\langle T(\rho) \rangle_Y$: for sufficiently large values of Y, this averaged quantity loses any memory of the shape of the event–by–event front (in particular, of geometric scaling), since it is dominated by *front dispersion* [38].

Specifically, starting with an unique initial condition at $Y = 0$, a stochastic evolution generates an *ensemble of fronts* at rapidity Y, where the individual fronts have more or
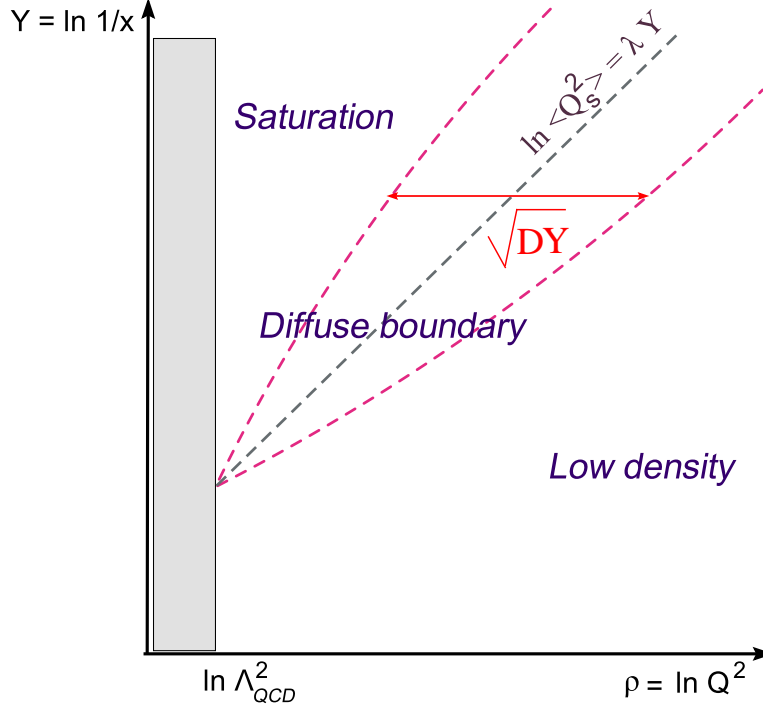
Fig. 2. *The diffusive saturation boundary generated by the evolution with fluctuations.*

less the same shape (cf. Eq. (3.4)) but differ from each other by a translation. That is, the ensemble can be described by treating the position ρ_s of a front as a *random variable*, which on the basis of the correspondence with statistical physics can be argued to have a Gaussian probability distribution [37, 53, 62] :

$$P_Y(\rho_s) = \frac{1}{\sqrt{\pi}\sigma} \exp\left[-\frac{(\rho_s - \langle\rho_s\rangle)^2}{\sigma^2}\right]. \tag{3.8}$$

with

$$\langle\rho_s\rangle = \lambda\bar{\alpha}_s Y, \qquad \text{and} \qquad \sigma^2 \equiv 2\left(\langle\rho_s^2\rangle - \langle\rho_s\rangle^2\right) = D_{\text{fr}}\bar{\alpha}_s Y, \tag{3.9}$$

where the *average front velocity* λ and the *front diffusion coefficient* D_{fr} are analytically known only in the limit $\alpha_s^2 \to 0$: λ is then given by Eq. (3.5), whereas D_{fr} scales as

$$D_{\text{fr}} \simeq \frac{\mathcal{D}}{\ln^3(1/\alpha_s^2)} \qquad \text{when} \qquad \alpha_s^2 \to 0, \tag{3.10}$$

with a coefficient $\mathcal{D}$ that has been recently computed in Ref. [62]. Since the parameters λ and D_{fr} not known for realistic values of α_s, in what follows we shall treat them as *free parameters*. In fact, rather than ρ and Y, it will be more convenient to work with the scaled variables $z \equiv \rho - \langle\rho_s\rangle$ and σ.

We see that, as a consequence of fluctuations, the saturation boundary become *diffuse*, within a radius $\sigma \propto \sqrt{Y}$ around the *average* saturation line $\langle\rho_s\rangle$ (see Fig. 2). This mechanism should not be confused with the BFKL diffusion, which applies to the individual fronts, and which becomes anyway inoperative for sufficiently large rapidities $Y > Y_{\text{form}}$,

as we have seen. The dispersion in the saturation boundary rather means that, in the vicinity of the average saturation line $\langle \rho_s \rangle$, the hadron wavefunction is the site of wild fluctuations in the gluon density. When probing the hadron (say, with an external dipole) on a resolution scale ρ within the diffusive radius ($|\rho - \langle \rho_s \rangle| \lesssim \sigma$), one can either find a 'black spot' — a gluon configuration with saturation scale $\rho_s \geq \rho$, which will completely absorb the projectile —, or a 'white spot' — a configuration having $\rho_s \ll \rho$, for which the dipole will emerge unscattered —, or any intermediate nuance of 'grey'.

Although this picture has been obtained by working at a fixed impact parameter, it can be easily extended to a picture of the target in impact parameter space, under the assumption that the high–energy evolution is *quasi–local* in b (as argued in Refs. [37, 38]). Then, the evolutions at different points b proceed (quasi)independently from each other and randomly generate any of the fronts which compose the statistical ensemble at Y. Accordingly, the average over the ensemble of fronts is tantamount to an average over all the impact parameters within the target area. We see that, even if one starts with homogeneous initial conditions at $Y = 0$, the target becomes highly inhomogeneous at large Y, as a consequence of (gluon–number) fluctuations in the course of the evolution. These inhomogeneities can be probed by a dipole projectile: A dipole with size r explores an area $\sim r^2$ around its impact parameter b. Because of the strong dispersion in the ensemble of fronts at large Y, a small dipole with $\rho \gg \langle \rho_s \rangle$ can 'see' either 'black spots', or 'white', or 'grey', depending upon its impact parameter. This is illustrated in Figs. 3.a and b.

The crucial feature about this situation is the fact that, for sufficiently large values of Y (such that $\sigma \gg 1$), the 'black spots' completely dominate the average dipole amplitudes [38] up to very large values of $\rho \gg \langle \rho_s \rangle$, that is, including in the 'weak scattering regime' where $\langle T(\rho) \rangle_Y \ll 1$. When this happens, the contribution of the 'grey spots' is negligible, so the hadron appears to the external dipole as *either black, or white* (see Fig. 3.c) : mostly black when $\rho \ll \langle \rho_s \rangle$, but mostly white in the opposite situation where $\rho \gg \langle \rho_s \rangle$. In fact, for $\sigma \gg 1$ and at all the points deeply inside the diffusion radius ($|\rho - \langle \rho_s \rangle| \ll \sigma$), the proportions of black and white are almost the same, so the average scattering amplitude is simply one–half ! But the dominance of the black spots actually extends up to much larger values of ρ, well outside the diffusive radius, namely so long as $\rho - \langle \rho_s \rangle \ll \sigma^2$.

To understand how this radically new physical picture arises, consider the average dipole amplitude, which in the present context is obtained as an average over the statistical ensemble of fronts, with weight function (3.8):

$$\langle T(\rho) \rangle_Y = \int_{-\infty}^{\infty} \mathrm{d}\rho_s \, P_Y(\rho_s) \, T(\rho - \rho_s), \tag{3.11}$$

with $T(\rho - \rho_s)$ the single–event front in Eq. (3.4). (Higher–point correlations can be similarly computed.) The values of ρ_s which dominate this convolution depend upon the competition between σ (the width of the Gaussian distribution of the fronts) and $1/\gamma$, with $\gamma \sim \mathcal{O}(1)$, which characterizes the exponential decay of the individual fronts. Specifically:

i) When $\sigma \ll 1/\gamma$ (the situation in the early stages of the evolution), the Gaussian ensemble is strongly peaked around the average front, hence the average amplitude retains
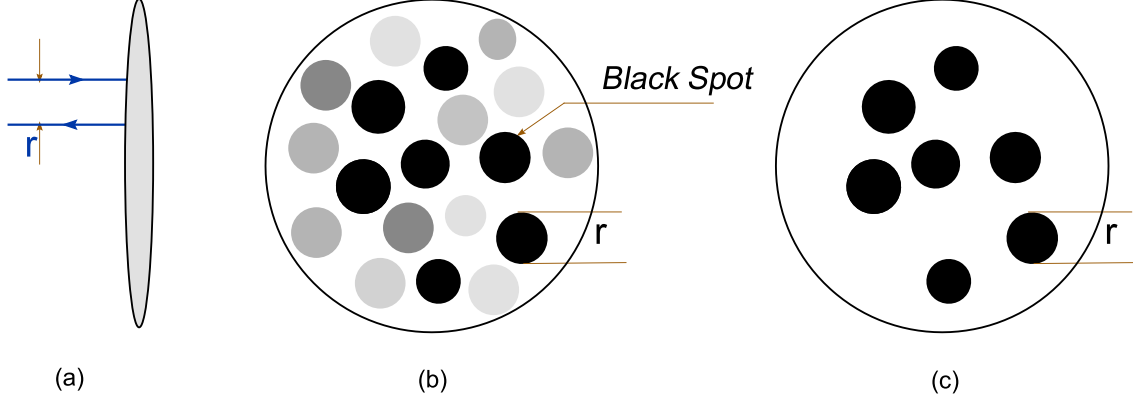
Fig. 3. *Dipole–hadron scattering in the fluctuation–dominated regime at $\sigma^2 \gg 1$. (a) a view along the collision axis; (b) a transverse view of the hadron, as 'seen' by a small dipole impinging at different impact parameters; (c) the simplified, black&white, picture of the hadron which is relevant for the average dipole amplitude.*

the single event profile:

$$\langle T(\rho) \rangle_Y \approx T(\rho - \langle \rho_s \rangle), \tag{3.12}$$

and thus shows *geometric scaling.*

ii) When $\sigma \gg 1/\gamma$ (the situation at sufficiently high energy), then for all the values of ρ such that $z \equiv \rho - \langle \rho_s \rangle \ll \gamma \sigma^2$, the average amplitude is dominated by 'black spots', i.e., by configurations with $\rho_s \geq \rho$, which look black ($T = 1$) on the resolution scale of the projectile. Note that, for large $\rho > \langle \rho_s \rangle$, such configurations are relatively rare, yet they dominate the convolution (3.11) since the contributions $T(\rho - \rho_s)$ of the typical configurations (for which $\rho_s \sim \langle \rho_s \rangle$) are exponentially suppressed. One then finds

$$\langle T(\rho) \rangle_Y \simeq \int_{\rho}^{\infty} d\rho_s \, P_Y(\rho_s) = \frac{1}{2} \operatorname{Erfc}\left(\frac{z}{\sigma}\right) \qquad \text{for} \quad -\infty < z \ll \gamma \sigma^2, \tag{3.13}$$

where the neglected terms are suppressed by, at least, one power of $1/\sigma$ and/or z/σ^2. (Note that we often use the fact that $\gamma \sim O(1)$ to simplify the parametric estimates.) Eq. (3.13) involves the complementary error function,

$$\operatorname{Erfc}(x) \equiv \frac{2}{\sqrt{\pi}} \int_{x}^{\infty} dt \, e^{-t^2} = \begin{cases} 2 - \dfrac{\exp(-x^2)}{\sqrt{\pi}\,|x|} & \text{for } x \ll -1 \\ 1 & \text{for } |x| \ll 1 \\ \dfrac{\exp(-x^2)}{\sqrt{\pi}x} & \text{for } x \gg 1. \end{cases} \tag{3.14}$$

As anticipated, the average amplitude at high energy is approximately constant, $\langle T(\rho) \rangle_Y \approx 1/2$, within the large interval $|z| \ll \sigma$ around the average saturation line. Moreover, within the whole validity region of the approximation (3.13), i.e., for $z \ll \sigma^2$, the amplitude shows *diffusive scaling* : it depends upon ρ (or r) and Y only via the single variable
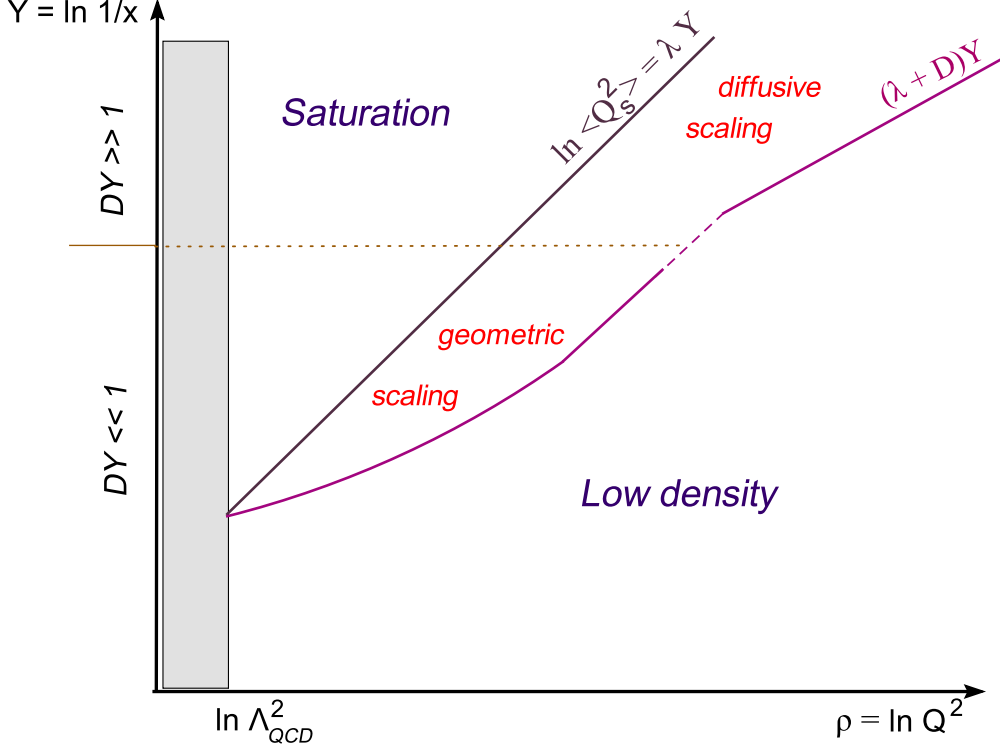
15

Fig. 4. *A 'phase–diagram' for the high–energy evolution with Pomeron loops. Shown are the average saturation line and the approximate boundaries of the scaling regions at large values of $\rho \sim \ln Q^2$ (with the simplified notations $\langle \rho_s \rangle = \lambda Y$ and $\sigma^2 = DY$). Note the gradual transition with increasing Y from geometric scaling at intermediate energies ($DY \ll 1$) to diffusive scaling at very high energies ($DY \gg 1$). This transition can be more quantitatively studied on Eq. (4.3).*

$$\tau \equiv \frac{z}{\sigma} \equiv \frac{\rho - \langle \rho_s \rangle}{\sigma} \equiv \frac{\ln(1/r^2 \langle Q_s^2 \rangle)}{\sigma} . \tag{3.15}$$

The physical regions for high–energy evolution in the kinematical plane $\rho - Y$ are illustrated in Fig. 4. The boundary of the geometric scaling window at large ρ follows from the discussion after Eq. (3.4). As for the diffusive scaling window, this extends up to $\rho_{\max} \simeq \langle \rho_s \rangle + \sigma^2 = (\lambda + D_{\mathrm{fr}}) \bar{\alpha}_s Y$, cf. Eq. (3.13). A more complete expression for the average amplitude which interpolates between these various regions will be presented in the next section (see Eq. (4.3)). Here, we would like to focus on the high–energy amplitude (3.13), which exhibits some other remarkable properties:

For relatively large $\rho \gg \langle \rho_s \rangle$ such that $z \gg \sigma$ (with $z \ll \sigma^2$ though), this function decreases as a Gaussian in z, rather than as an exponential. Thus, within a rather wide window at high Q^2, whose width is increasing with Y (see Fig. 4), the scattering is weak, yet there is *no 'twist–expansion'* — i.e., no expansion in powers of $r^2 \sim 1/Q^2$ — for the scattering amplitude. 'Color transparency', meaning that $\langle T(\rho) \rangle \propto \mathrm{e}^{-\rho}$, is eventually recovered, but only for very large $z \gtrsim \sigma^2$ (cf. Eq. (4.3)). Furthermore, the amplitude (3.13) shows *no 'Pomeron'–like growth* — i.e., no power–like increase with Y at fixed ρ.

Such properties might look curious, but in fact they are easy to understand in the present context: Both color transparency and the power–like increase with Y are properties of

the scattering between the projectile dipole and a *dilute* gluon configuration in the target. But as already explained, Eq. (3.13) rather describes the scattering off *dense* gluon configurations, for which the individual amplitudes have already reached the unitarity limit $T = 1$. When varying ρ or Y, we modify the composition of the statistical ensemble which is probed by the scattering, but the average amplitude changes only slowly.

It is important to emphasize that the functional form (3.13) of the high–energy amplitude is *extremely robust*, as it follows from very few and general physical assumptions: the facts that the amplitude $T(r)$ saturates the unitarity limit $T = 1$ for sufficiently large dipole sizes r and vanishes like a power of r when $r \to 0$, and that the gluon–number fluctuations in the target lead to a dispersion in the ensemble of fronts, which increases with Y. By the same arguments, this result is *universal* : it is insensitive to the initial conditions at low energy and also to the details of the high–energy evolution. The latter matter only for the calculation of the parameters λ and D_{fr}, or, more generally, of the Y–dependencies of the average saturation scale $\langle \rho_s(Y) \rangle$ and of the front dispersion $\sigma(Y)$.

By using Eq. (3.13) within the dipole factorization scheme for DIS, we have been able to estimate (in a previous work which also included Y. Hatta and D. N. Triantafyllopoulos [45]) the high–energy limit of the inclusive and diffractive DIS cross–sections, and thus demonstrate that all the remarkable properties discussed above in relation with the dipole amplitude do also transmit to these cross–sections. Returning to the problem of interest for us here — namely, gluon production in onium–hadron collisions at forward rapidity — it seems natural to anticipate that these properties will show up in this context too, since the corresponding cross–section (2.2) is again related to the dipole amplitude. But a closer inspection of Eq. (2.2) may shed serious doubts on this conclusion: the 'generalized gluon occupation factor' defined in Eq. (2.7), and which is a building block of the cross–section (2.2), involves the (second order) *derivative* of the dipole amplitude. When taking this derivative on the convolution (3.11), we kill the contribution of the fronts which are at saturation in the statistical ensemble (the 'black spots'), because for them $T = 1$. Rather, the whole non–trivial contribution to this derivative arises from the *tails* of the individual fronts. Thus, clearly, gluon production is dominated by a different physics as compared to DIS, and one may wonder whether this physics is universal at high energy, and whether it can be computed within the present formalism. The answer to both questions turns out to be 'yes', as we shall argue in the next section.

4   The generalized gluon distribution

We start with Eq. (2.7) which is rewritten as (after performing the angular integration)

$$
\Phi(k, Y) = \int_0^\infty \mathrm{d}r\, r\, J_0(kr) \frac{1}{r} \frac{\partial}{\partial r} \left(r \frac{\partial}{\partial r} \left\langle T_{gg}(r) \right\rangle_Y \right)
$$
$$
= 2 \int \mathrm{d}\rho\, J_0\!\left(k r_0 \mathrm{e}^{-\rho/2} \right) \frac{\partial^2}{\partial \rho^2} \left(2 \left\langle T(\rho) \right\rangle_Y - \left\langle T^2(\rho) \right\rangle_Y \right), \tag{4.1}
$$

where $\rho \equiv \ln(r_0^2/r^2)$ and we have used Eq. (2.9) to express the second line in term of $q\bar{q}$ dipole amplitudes alone. As explained at the end of the previous section, the derivative

$\partial_\rho \langle T(\rho) \rangle_Y$ is controlled by the tails of the individual fronts in the statistical ensemble. Hence, in order to compute this quantity, one needs to evaluate Eq. (3.11) with a complete profile for the single–event front, which includes a model for the tail. However, we shall shortly argue that the precise shape of the tail is unimportant in the kinematic range of interest and, moreover, the required derivatives can be simply obtained by differentiating Eq. (3.13) ! This seems paradoxical, since Eq. (3.13) has been *a priori* obtained by neglecting the tails altogether ! This paradox is resolved by observing that the dominant contributions to these derivatives are actually given by the *end points* of the tails towards the saturation region (that is, by $\rho \sim \rho_s$).

In order to show this and also compute $\partial_\rho \langle T(\rho) \rangle_Y$ to the desired accuracy, we shall use the following, simplified, profile for a single front (compare to Eq. (3.4))

$$
T(\rho) = \begin{cases} 1 & \text{for } \rho < \rho_s \\ e^{-\gamma(\rho-\rho_s)} & \text{for } \rho \geq \rho_s\,, \end{cases} \tag{4.2}
$$

with generic $\gamma \sim \mathcal{O}(1)$. A simple calculation yields (with $z \equiv \rho - \langle \rho_s \rangle$)

$$
\langle T(\rho) \rangle_Y = \frac{1}{2}\,\mathrm{Erfc}\left(\frac{z}{\sigma}\right) + \frac{1}{2}\exp\left(\frac{\gamma^2\sigma^2}{4} - \gamma z\right)\left[2 - \mathrm{Erfc}\left(\frac{z}{\sigma} - \frac{\gamma\sigma}{2}\right)\right]. \tag{4.3}
$$

The first term is the same as in Eq. (3.13) and comes from the saturation piece of the single front (4.2), while the second term comes from the exponential tail in Eq. (4.2). Incidentally, the previous results in Eqs. (3.12) and (3.13) can be easily recovered by expanding Eq. (4.3) in the corresponding limits. The corresponding expression for $\langle T^2(\rho) \rangle_Y$ is obtained by replacing $\gamma \to 2\gamma$ into Eq. (4.3).

At this level, it is straightforward to compute the required derivatives by acting with $\partial_\rho \equiv \partial_z$ on Eq. (4.3). However, it is more instructive for what follows to compute at least the first derivative *before* performing the Gaussian average over ρ_s, that is, by first differentiating the single–event profile (4.2) and then averaging. By using

$$
\partial_\rho T(\rho) = -\gamma\,\Theta(\rho-\rho_s)\,e^{-\gamma(\rho-\rho_s)}, \tag{4.4}
$$

which implies

$$
\partial_\rho \langle T(\rho) \rangle_Y = -\gamma \int_{-\infty}^{\rho} \mathrm{d}\rho_s\, e^{-\gamma(\rho-\rho_s)}\, P_Y(\rho_s), \tag{4.5}
$$

it becomes manifest that the derivative is fully controlled by the tail, as anticipated. But Eq. (4.5) also shows that the contributions of the fronts with $\rho_s \ll \rho$ are exponentially suppressed; so, unless ρ is too different from $\langle \rho_s \rangle$ (in such a way that the probability $P_Y(\rho_s \sim \rho)$ be suppressed even stronger !), the integral in Eq. (4.5) is dominated by ρ_s close to the upper limit, within a distance $1/\gamma$ from it. This yields the following estimate

$$
\partial_\rho \langle T(\rho) \rangle_Y \approx -P_Y(\rho_s = \rho) = -\frac{1}{\sqrt{\pi}\sigma}\,e^{-\frac{z^2}{\sigma^2}} \qquad \text{for} \qquad |z| \ll \sigma^2, \tag{4.6}
$$

18

which can be confirmed via a direct calculation based on Eq. (4.3). Remarkably, this result coincides with the first derivative of the 'black spots' approximation for $\langle T(\rho)\rangle_Y$, Eq. (3.13).

Thus, as anticipated, the ρ–derivative of the average dipole amplitude is dominated by those fronts in the ensemble for which the position ρ_s of the front is of the order of the dipole resolution scale. Because of that, the result (4.6) is *robust and universal* (i.e., insensitive to the details of the evolution), except possibly for its overall normalization, which is not fully under control in the present approximations (since this depends upon the precise approach of an individual front towards saturation). The same conclusions hold, of course, for the second–order derivative ∂_ρ^2, which can be computed either from Eq. (4.3), or directly from Eq. (3.13), with the following result:

$$\frac{\partial^2}{\partial\rho^2}\,\langle T(\rho)\rangle_Y \;\simeq\; \frac{2\,z}{\sqrt{\pi}\sigma^3}\;\mathrm{e}^{-\frac{z^2}{\sigma^2}} \qquad \text{for} \qquad |z|\ll\sigma^2\,. \tag{4.7}$$

Since the estimates (4.6) and (4.7) are independent of γ, it is clear that they identically hold for the corresponding derivatives of $\langle T^2(\rho)\rangle_Y$ as well. This is also in agreement with the fact that, within the validity range of Eq. (3.13), all the N–body dipole amplitudes coincide with each other:

$$\langle T(\rho)\rangle \;\simeq\; \langle T^2(\rho)\rangle \;\simeq\; \langle T^N(\rho)\rangle \;\approx\; \frac{1}{2}\,\mathrm{Erfc}\left(\frac{z}{\sigma}\right) \quad \text{for} \quad \sigma\gg 1 \quad \text{and} \quad z\ll\sigma^2\,. \tag{4.8}$$

The universal functions which yield the dipole amplitude $\langle T(\rho)\rangle_Y$ and its first two derivatives (appropriately rescaled by factors of σ in order to exhibit diffusive scaling) in this high–energy regime are shown in Fig. 5.

To complete our calculation of the generalized gluon distribution, we need to evaluate the Fourier transform in Eq. (4.1). We shall first give an analytic estimate, based on Eq. (4.7), for the dominant behaviour at high energy, and then verify this estimate, and also study a wider kinematical range, via a numerical calculation using the more complete expression (4.3) for the average dipole amplitude.

Let us start by introducing some new notations, which will be useful in what follows:

$$Z \;\equiv\; \ln\frac{k^2}{\langle Q_s^2\rangle}\,, \qquad \eta \;\equiv\; \ln\frac{1}{r^2 k^2} \;=\; \ln\frac{1}{r^2\langle Q_s^2\rangle} \;-\; \ln\frac{k^2}{\langle Q_s^2\rangle} \;=\; z - Z\,, \tag{4.9}$$

We shall now deduce an analytic estimate for the 'occupation factor' $\Phi(k,Y) \equiv \Phi(Z,Y)$ valid in high energy regime at $\sigma\gg 1$ and for transverse momenta k within a wide interval around the average saturation momentum $\langle Q_s(Y)\rangle$, specified by $|Z|\ll\sigma^2$. By inspection of the integrand in Eq. (4.1), we expect the integral to be dominated by dipole sizes $r\sim 1/k$ (or $z\sim Z$), for which Eq. (4.7) applies: Indeed, the Fourier transform restricts the integration to $kr\lesssim 1$ (or $z\gtrsim Z$), but the extremely small values $r\ll 1/k$ (or very large $z\gg Z$) are suppressed by the Gaussian decay of the dipole amplitude, cf. Eq. (4.7).

After also using the property $2\langle T\rangle - \langle T^2\rangle = \langle T\rangle$, cf. Eq. (4.8), and the new notations introduced in Eq. (4.9), Eq. (4.1) can be rewritten as
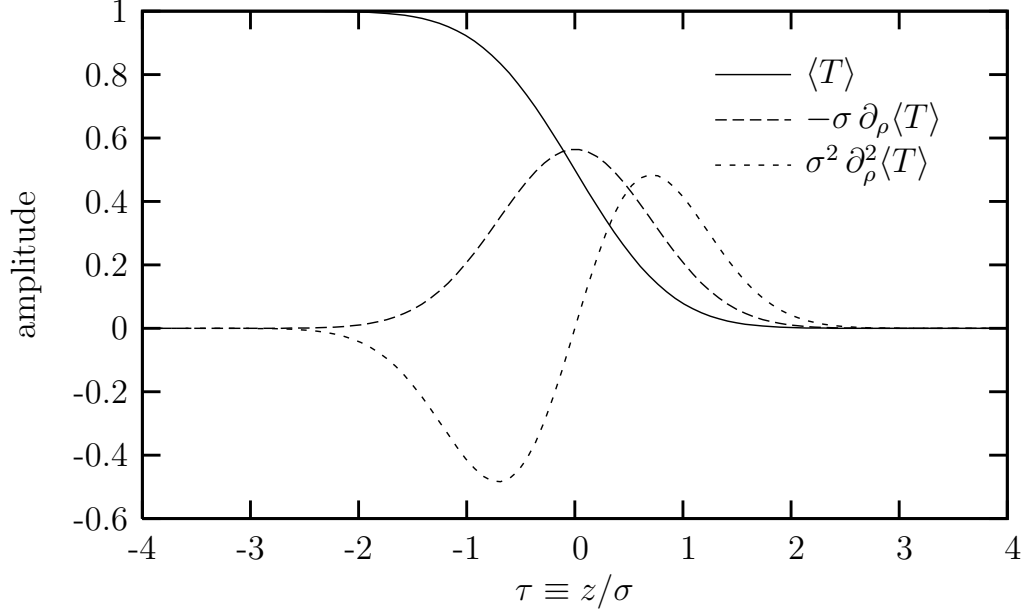
Fig. 5. *The average dipole amplitude in the 'black spots' approximation, Eq. (3.13), together with its first and second derivatives (scaled by appropriate powers of σ in such a way to exhibit diffusive scaling) are represented as functions of the respective scaling variable τ, Eq. (3.15).*

$$\Phi(Z,Y) = 2 \int d\eta \, J_0\left(e^{-\eta/2}\right) \frac{\partial^2}{\partial \eta^2} \Big\langle T(\eta + Z) \Big\rangle_Y \tag{4.10}$$

where the average amplitude is viewed as a function of $z = \eta + Z$ — the natural variable in the r.h.s. of Eq. (4.7). The Bessel function $J_0(x)$ is oscillating for large values of its argument x, with the amplitude of the oscillations rapidly decreasing when increasing x. Hence, the dominant contribution to the above integral is given by the interval between $x = 0$ and the first zero x_0 of the Bessel function (i.e., from $\eta = \eta_0$, with $e^{-\eta_0/2} \equiv x_0$, to $\eta \to \infty$), within which $J_0(x) \approx$ const. This yields the following estimate

$$\Phi(Z,Y) \approx \frac{1}{\sigma^3} \int\limits_{\eta_0}^{\infty} d\eta \, (\eta + Z) \, e^{-\frac{(\eta+Z)^2}{\sigma^2}}$$

$$= \frac{1}{\sigma} e^{-\frac{(\eta_0+Z)^2}{\sigma^2}} \approx \frac{1}{\sigma} e^{-\frac{Z^2}{\sigma^2}} \qquad \text{for} \quad \sigma \gg 1 \quad \text{and} \quad 1 \ll |Z| \ll \sigma^2 \,, \tag{4.11}$$

up to some numerical fudge factor. (The precise position of the center of the Gaussian is not really under control here, hence the restriction to $|Z| \gg 1$.)

Eq. (4.11) is essentially the same as the Gaussian probability distribution of the fronts, Eq. (3.8). This result can be physically understood as follows: $\Phi(Z,Y)$ with $Z \equiv \ln(k^2/\langle Q_s^2 \rangle)$ is the *average* 'gluon occupation factor', as obtained after averaging the corresponding *event–by–event* quantity with the Gaussian probability (3.8). In turn, the event–by–event 'occupation factor' $\Phi_{\text{event}}(k, Y)$ is computed as the appropriate Fourier transform, cf. Eq. (2.7), of the dipole amplitude T in a single event [7], Eq. (3.4). The result of this cal-

---

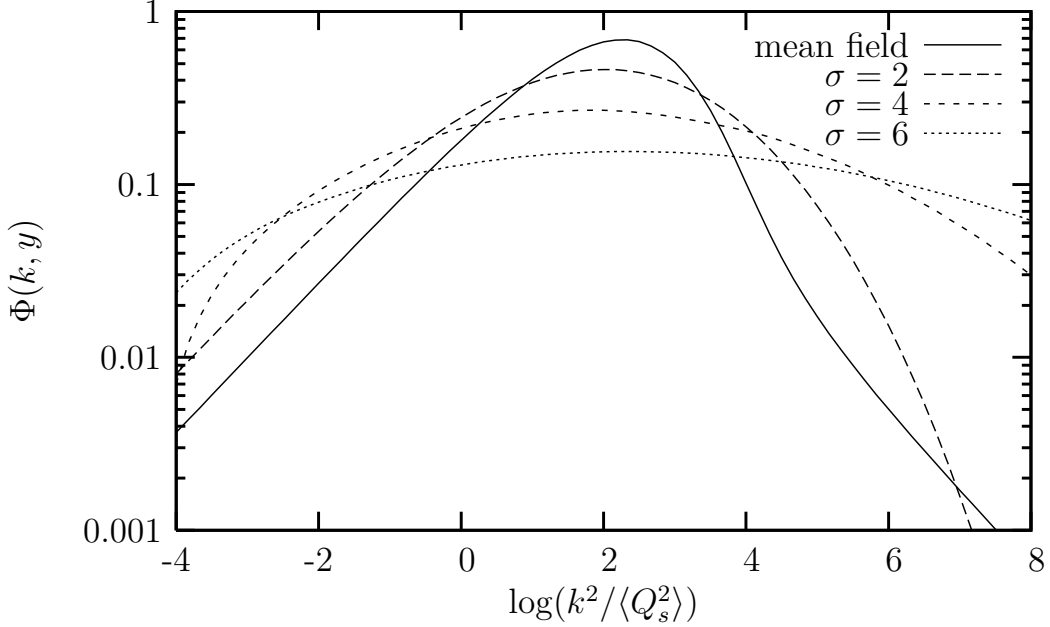[7] Strictly speaking, one cannot use a piecewise interpolation, so like Eq. (3.4), in the calculation

Fig. 6. *The average 'gluon occupation factor' obtained by numerical integration in Eq. (4.1) with the average dipole amplitude taken from Eq. (4.3) (with $\gamma = 1$) for $\sigma \geq 2$. For comparison, we also show the corresponding mean field curve obtained with the McLerran–Venugopalan model for the dipole amplitude. Note the flattening of the curve with increasing σ: this demonstrates the rapid breakdown of geometric scaling through fluctuations when increasing the energy.*

culation is well known from previous studies based on the mean field approximation (see, e.g., Ref. [6]) — namely, one finds that the single–event 'occupation factor' vanishes as k^2 at small $k \ll Q_s$ and it approaches the bremsstrahlung spectrum $\propto 1/k^2$ at large $k \gg Q_s$. In logarithmic units, with $\rho \equiv \ln(k^2 r_0^2)$, $\Phi_{\text{event}}(\rho, Y) \sim \mathrm{e}^{-|\rho - \rho_s|}$ is strongly peaked near $\rho = \rho_s$, and thus it behaves almost like a δ–function when averaged over ρ_s with a Gaussian probability with a large width $\sigma \gg 1$. This explains the result in Eq. (4.11). Note that the latter ceases to apply when $|Z| \gtrsim \sigma^2$, i.e., for momenta k which are very much smaller, or very much larger, than the average saturation momentum; but in that case, we expect to recover the standard exponential (in ρ) behaviour, namely $\Phi \sim \mathrm{e}^{-|\rho - \langle \rho_s \rangle|}$.

This discussion allows us to put the results in Sect. 3 in a somewhat wider physical perspective: The results of the high–energy evolution with Pomeron loops can be visualized directly in terms of the (unintegrated) gluon distribution in the hadron, independently of the problem of the scattering. This perspective is consistent with the original derivation of the Pomeron loop equations [38, 39], in which the high–energy evolution was described as the color–glass evolution of the target wavefunction.

Note the contrast between the event–by–event 'occupation factor' $\Phi_{\text{event}}(k, Y)$, which is strongly peaked at a transverse momentum k of the order of the saturation scale Q_s in

---

of a Fourier transform, since the discontinuities in the higher derivatives would introduce spurious oscillations. Rather, to that purpose one needs a smooth approximation to $T(r)$ so like the McLerran–Venugopalan model [16] or the BK solution. Within such approximations, one finds indeed an 'occupation factor' $\Phi_{\text{event}}(k, Y)$ with the behaviour discussed in the text [6, 8, 9, 30].
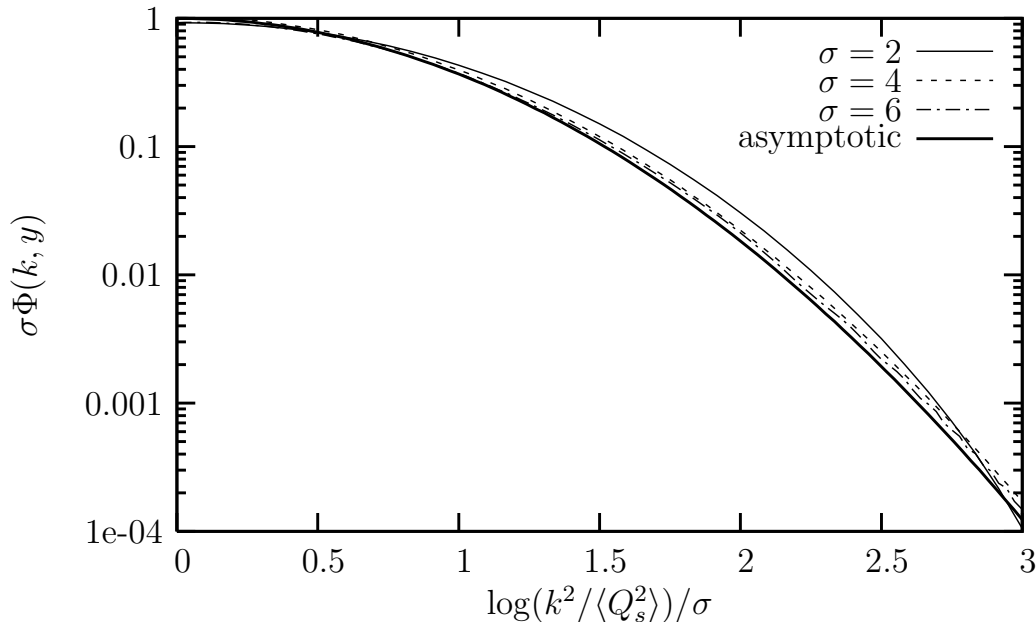
21

Fig. 7. *The results corresponding to $\sigma \geq 2$ in Fig. 6 are redisplayed as a function of the diffusive scaling variable $\tau \equiv Z/\sigma$. One can thus appreciate the rapid onset of the scaling behaviour when increasing σ (or Y). The asymptotic curve is the Gaussian in the r.h.s. of Eq. (4.11).*

that event, and its expectation value $\Phi(k, Y)$, which at large Y has only a mild peak at $k \sim \langle Q_s(Y) \rangle$. This behaviour is illustrated in Fig. 6 which shows the quantity $\Phi(Z, Y)$ obtained by numerical integration in Eq. (4.1) with the average dipole amplitude taken from Eq. (4.3). As manifest on this figure, the dispersion in the gluon distribution increases rapidly with σ (hence, with Y), leading to the breakdown of geometric scaling. The large–σ behaviour is in qualitative agreement with the analytic estimate (4.11). To more precisely test the latter, notice that, according to Eq. (4.11), the function $\sigma\Phi(Z, Y)$ should exhibit diffusive scaling at sufficiently high energy. In order to check this, we have redisplayed the numerical results from Fig. 6 as a function of the scaling variable $\tau \equiv Z/\sigma$: as manifest on Fig. 7, the diffusive scaling emerges indeed (and quite fast !) when increasing σ.

5 The cross–section for gluon production

We are finally in a position to complete our original objective in this paper, namely the calculation of the differential cross–section (2.3) for forward gluon production in onium–hadron scattering at high energy. By using the expression (4.3) for the average dipole–target amplitude, together with the BFKL solution (2.4) for the dipole number density in the projectile, it is in principle possible to (numerically) evaluate the integral in Eq. (2.3) for arbitrary values of its external variables. However, one can always gain more insight via an analytic estimate, and this can be indeed obtained in the kinematical regime of interest for us here, namely the regime in which the Pomeron loop effects are most visible on this cross–section.

Specifically, this regime is characterized by large values for the total rapidity Y and

also for the pseudo–rapidity η of the produced gluon (but such that the difference $y_1 = Y/2 - \eta$ remains relatively small, cf. Eq. (2.1)), and also by relatively large values for the transverse momentum $k \equiv k_\perp$ of the produced gluon, in the vicinity of the average saturation momentum in the target $\langle Q_s^2(y_2) \rangle$. The most interesting conditions are when $\sigma^2 \equiv D_{\mathrm{fr}} \bar{\alpha}_s y_2 \gg 1$ and $|\ln(k^2/\langle Q_s^2 \rangle)| \ll \sigma^2$, since in these conditions we probe the fluctuation–dominated regime in the target wavefunction, cf. Fig. 4. (Here and from now on, the quantities $\langle Q_s^2 \rangle$ and σ will always refer to the target, hence they are evaluated at a rapidity $y_2 = Y/2 + \eta$.)

Under these assumptions, the convolution in Eq. (2.3) simplifies considerably, as is best seen on the $k_\perp$–factorized version of this cross–section, Eq. (2.5): Given the large asymmetry between the evolutions of the projectile and respectively the target (recall that $y_2 \gg y_1$), the interesting values for the external momentum k^2 are much larger than the momentum scale $Q_p^2(y_1) \sim (1/r_0^2) e^{\lambda \bar{\alpha}_s y_1}$ which is generated in the projectile wavefunction by its own high–energy evolution. ($Q_p^2(y_1)$ is the saturation scale of the projectile, and effectively acts as an infrared cutoff[8] in the integral over p in Eq. (2.5).) When this happens, the integral in Eq. (2.5) is dominated by momenta p logarithmically distributed within the range $Q_p^2(y_1) \ll p^2 \ll k^2$; in the leading logarithmic approximation w.r.t. the transverse logarithm $\ln(k^2/Q_p^2)$, the result can be estimated as

$$\frac{\mathrm{d}\sigma}{\mathrm{d}\eta \mathrm{d}^2 k \mathrm{d}^2 b} \approx \frac{\bar{\alpha}_s}{k^2} \Phi(k, y_2) \int^{k^2} \frac{\mathrm{d}^2 \boldsymbol{p}}{(2\pi)^2} \varphi(\boldsymbol{p}, y_1) \propto \frac{1}{k^2} \Phi(k, y_2) x_1 G_p(x_1, k^2), \qquad (5.1)$$

where $x_1 G_p(x_1, k^2)$ is the integrated gluon distribution in the projectile evaluated for a longitudinal momentum fraction $x_1 = e^{-y_1}$ and a transverse resolution (or momentum cutoff) k^2. More precisely, it can be checked that the estimate (5.1) holds under the following conditions:

$$-\sigma \ll Z \equiv \ln \frac{k^2}{\langle Q_s^2 \rangle} \ll \sigma^2 \qquad \text{and} \qquad \ln \frac{k^2}{Q_p^2} \gg \sigma. \qquad (5.2)$$

The first inequality ($Z \gg -\sigma$) is necessary to ensure that the contribution of the relatively large momenta $p \gg k$ to the integral in Eq. (2.5) is indeed subleading in the regime where $\Phi(p, y_2)$ is given by Eq. (4.11). The second inequality ($Z \ll \sigma^2$) ensures the validity of the approximation (4.11) for $\Phi(k, y_2)$. Finally, the third inequality is not really independent — it automatically follows from the previous conditions together with the fact that $\ln(\langle Q_s^2 \rangle / Q_p^2) \propto \eta$ grows much faster with η than $\sigma \sim \sqrt{\eta}$ — but it is nevertheless shown here to emphasize that the leading–twist approximation for the projectile requires the stronger condition $\ln(k^2/Q_p^2) \gg \sigma$ rather than just the usual one $\ln(k^2/Q_p^2) \gg 1$.

Eq. (5.1) is recognized as the *collinear factorization* of the cross–section for gluon production; this is valid, as expected, at sufficiently large k. Note that this formula still involves the *unintegrated* gluon distribution of the target, $\Phi(k, y_2)$, which is moreover computed in a regime where the saturation effects are important. Thus, although it looks familiar, the

---

[8] Indeed, this is the scale at which there is a turnover in $\varphi(\boldsymbol{p}, y_1)$ from the bremsstrahlung spectrum $\propto 1/p^2$ at large momenta to the saturation spectrum $\propto p^2$ at low momenta.

collinear factorization in Eq. (5.1) emerges here in a less familiar context: the one in which the leading–twist approximation applies to the projectile, but not also to the target.

Strictly speaking, the projectile distribution $x_1 G_p(x_1, k^2)$ which enters Eq. (5.1) should be computed in the double–logarithmic approximation (DLA) — the approximation which resums both the high–energy logarithms $\ln(1/x_1)$ and the transverse ones $\ln(k^2 r_0^2)$ —, since it emerges from a $k_\perp$–factorization at high energy. But this is not important here since, irrespective of the actual approximation which is used to compute this function (DGLAP or DLA), the result is anyway slowly varying with k^2 as compared to the other functions which appear in the r.h.s. of Eq. (5.1).

According to Eq. (5.1), the spectrum of the produced gluon is proportional to the gluon occupation factor in the target $\Phi(k, y_2)$ that we have already computed (in the high–energy regime of interest) in the previous section. To better appreciate the modifications introduced by Pomeron loop effects, it is preferable to consider the distribution in $\ln k^2$:

$$\frac{\mathrm{d}\sigma}{\mathrm{d}\eta\,\mathrm{d}\ln k^2\,\mathrm{d}^2 b} \propto \Phi(k, y_2), \tag{5.3}$$

which is simply proportional to $\Phi(k, y_2)$. (We ignore the weak dependence of the projectile gluon distribution upon k^2.) One can then distinguish various physical regimes:

i) When k^2 is extremely high, so high that the saturation effects become completely negligible, the gluon occupation factor in the target takes its standard perturbative form, i.e., the bremsstrahlung spectrum (up to the effects of the DGLAP evolution, that we neglect here) :

$$\frac{\mathrm{d}\sigma}{\mathrm{d}\eta\,\mathrm{d}\ln k^2\,\mathrm{d}^2 b} \propto \frac{1}{k^2} \qquad \text{when} \qquad k^2 \ggg \langle Q_s^2 \rangle. \tag{5.4}$$

We use here the notation $k^2 \ggg \langle Q_s^2 \rangle$ to emphasize that, in the fluctuation–dominated regime at high energy ($\sigma^2 \gg 1$), this leading–twist result is recovered only for momenta so large as compared to $\langle Q_s^2 \rangle$ that the condition $Z \gtrsim \sigma^2$ is satisfied, with $Z \equiv \ln(k^2/\langle Q_s^2 \rangle)$.

For lower momenta, but still much larger than the (average) saturation momentum, we encounter *saturation* effects, which can be different depending upon the energy range at hand (see also Fig. 4) :

ii) For intermediate energies, such that $\sigma^2 \ll 1$, the effects of fluctuations are negligible and the BFKL evolution with saturation boundary conditions leads to *geometric scaling* at intermediate momenta, with an 'anomalous dimension' $\gamma_0 \approx 0.63$:

$$\frac{\mathrm{d}\sigma}{\mathrm{d}\eta\,\mathrm{d}\ln k^2\,\mathrm{d}^2 b} \propto \left(\frac{Q_s^2}{k^2}\right)^{\gamma_0} \qquad \text{when} \qquad Q_s^2 \ll k^2 \lesssim Q_g^2. \tag{5.5}$$

Here, we have written $\langle Q_s^2 \rangle \equiv Q_s^2$ (no fluctuations !) and used Q_g^2 to denote the upper boundary of the geometric scaling window. We have $Q_g^2 \equiv Q_s^2 \mathrm{e}^{z_g}$ where the exponent z_g grows like $z_g \sim \sqrt{y_2}$ in the early stages of the evolution (cf. Eq. (3.3)), and then get stuck at a value $z_g \sim L$ when $y_2 \gtrsim Y_{\text{form}}$ (cf. Eqs. (3.6)–(3.7)).

iii) For very high energies, such that $\sigma^2 \gg 1$, one enters the fluctuation–dominated regime, where the target occupation factor $\Phi(k, y_2)$ (cf. Eq. (4.11)), and hence the produced gluon spectrum (5.3), are dominated by 'black spots' with $Q_s \sim k$. Then, the average spectrum is a Gaussian in $Z \equiv \ln(k^2/\langle Q_s^2 \rangle)$ and shows *diffusive scaling* (after multiplication by a factor of σ) :

$$\frac{\mathrm{d}\sigma}{\mathrm{d}\eta \, \mathrm{dln}k^2 \, \mathrm{d}^2b} \propto \frac{1}{\sigma} \exp\left\{-\frac{Z^2}{\sigma^2}\right\} \qquad \text{when} \qquad -\sigma \ll Z \ll \sigma^2 \, . \tag{5.6}$$

Note the dramatic change in behaviour from the bremsstrahlung spectrum $1/k^2 \propto \mathrm{e}^{-Z}$, which is naively expected at high k^2, to the Gaussian spectrum (5.6), which at sufficiently high energy should prevail up to very large values of k^2, well above $\langle Q_s^2 \rangle$ (and also well below it, within the range indicated in the equation above).

6 Conclusion and perspectives

The main conclusion of this work is that forward particle production in proton–proton collisions at high energy represents an ideal laboratory to search for the new physics expected in QCD at very high energies. Indeed, the spectrum of the gluons produced at forward rapidities reflects quite faithfully the unintegrated gluon distribution in the highly evolved hadronic target, and thus is directly sensitive to new phenomena like gluon saturation and gluon–number fluctuations, which are expected to become important at high energy. The essential consequence of these phenomena is the fact that, up to relatively large transverse momenta — well above the *average* saturation momentum in the target wavefunction —, the cross–section for gluon production is dominated by *black spots*, i.e., rare gluon configurations with unusually large density, which are at saturation on the resolution scale of the produced gluon. And the distinctive signature of this behaviour, which should be its hallmark in the experimental results, is a new scaling law — the *diffusive scaling* —, which should eventually replace at sufficiently high energy the 'geometric scaling' behaviour currently observed in the small–x data at HERA and RHIC.

Both geometric scaling and diffusive scaling are exceptional phenomena, in that they represent consequences of saturation which manifest themselves at relatively large transverse momenta, well outside the saturation region — that is, in a region of the phase–space where one would naively expect the applicability of the linear, or 'leading–twist', evolution equations of perturbative QCD (DGLAP or BFKL). But although they are both hallmarks of saturation, these two types of scaling correspond to very different physical regimes, that they should unambiguously identify in the data :

- *Geometric scaling* occurs at *intermediate energies*, i.e., energies which are large enough for the saturation momentum Q_s to be a hard scale, yet low enough for the dispersion in the values of Q_s (as generated via gluon–number fluctuations at low density) to remain negligible ($\sigma \ll 1$, cf. Fig. 4). In that regime, 'geometric scaling' is simply the statement that the physics remains invariant along any line parallel to the saturation line $\rho_s(Y) = \lambda Y$. But the dynamics when increasing $\rho \equiv \ln k_\perp$ above ρ_s (i.e., when moving away from saturation) is still described by the leading–twist, BFKL, formalism.

25

- *Diffusive scaling*, on the other hand, represents the ultimate behaviour at *sufficiently high energy*, where the dispersion in the gluon configurations is very large ($\sigma \gg 1$) and the high–density fluctuations dominate the expectation values within a wide window around the *average* saturation line $\langle \rho_s(Y) \rangle$ — namely, so long as $|\rho - \langle \rho_s \rangle| \ll \sigma^2$. Within that whole window (which includes very large momenta $k_\perp \gg \langle Q_s \rangle$!), the leading–twist approximation breaks down and the cross–section for gluon production is controlled by the physics of saturation (similarly to the DIS cross–sections [45]).

Properties of the gluon distribution produced via a high–energy evolution, the geometric and diffusive scaling naturally transmit (within their respective ranges of existence) to the scattering amplitudes for external dipoles — the most direct probes of the gluon distribution in the target — and hence to all the processes, so like lepton–hadron DIS or *forward* gluon production in hadron–hadron collisions, which can be given a dipole factorization. On the other hand, the consequences of these phenomena on the particle production at *central* rapidities — and, more generally, on the *symmetric* collision between two highly–evolved hadrons — are presently unclear, since there is no general factorization scheme for the scattering between two hadronic systems which are both affected by saturation.

This problem becomes particularly acute in the high–energy regime where the Pomeron loop effects are important, because in that case we expect saturated gluon configurations to significantly contribute to scattering up to very large transverse momenta (at least, this is what we have seen to happen in DIS and for the forward gluon production), so the standard, collinear– or $k_\perp$–, factorization schemes fail to apply even at very large transverse momenta, well above the average saturation scale. It thus remains as an important open problem how to compute, e.g., gluon production at central rapidity in proton–proton scattering with Pomeron loops. It is tempting to conjecture that, within a wide kinematical range, this process should be dominated by black–spots–on–black–spots scattering, but this remains to be proven.

But further theoretical progress is also needed in the simpler case of the asymmetric, dilute–dense, collisions, as discussed in this paper and in Ref. [45]. The results presented here have been obtained via rather crude approximations, which rely on the correspondence between high–energy evolution in QCD and the reaction–diffusion process in statistical physics, but do not allow for a more detailed characterization of the QCD amplitudes. Although the qualitative conclusions which emerged in this way (like the dominance of black spots up to large transverse momenta or the diffusive scaling) are quite robust, as they follow from fundamental considerations, some other, equally important, properties — chiefly among them, the energy dependencies of the average saturation momentum and of its dispersion —, remain poorly understood and deserve further studies.

To make progress, one needs more complete (possibly numerical) solutions to the Pomeron loop equations of Ref. [38]; this would allow one not only to determine the parameters λ and $D_{\rm fr}$, but also to control the impact–parameter dependence of the amplitudes (to leading order accuracy in α_s and $1/N_c$). Furthermore, the previous experience with the next–to–leading–order (NLO) corrections in the context of saturation [23] shows that such corrections are quantitatively important for all but the asymptotically high energies. A NLO formalism including Pomeron loops is therefore highly desirable, but this looks quite difficult to achieve. (Already the generalization of the present, LO, equations to

generic values of N_c meets with serious, technical and conceptual, problems, in spite of some recent progress [41, 43, 44].) There should be nevertheless possible to estimate at least *some* NLO effects, like those of the running of the coupling or of imposing energy conservation in the evolution. Last but not least, in view of more realistic calculations of the (forward) hadronic yield, it would be interesting to include some more processes at partonic level, so like quark pair production, and also to complete the (generalized) collinear factorization, Eq. (5.1), with fragmentation functions for the produced partons.

Acknowledgments

References

[1] B. B. Back *et al.* [PHOBOS Collaboration], *Phys. Rev. Lett.* **91** (2003) 072302; S. S. Adler *et al.* [PHENIX Collaboration], *Phys. Rev. Lett.* **91** (2003) 072303; J. Adams *et al.* [STAR Collaboration], *Phys. Rev. Lett.* **91** (2003) 072304; I. Arsene *et al.* [BRAHMS Collaboration], *Phys. Rev. Lett.* **91** (2003) 072305.

[2] I. Arsene *et al.* [BRAHMS Collaboration], *Phys. Rev. Lett.* **93** (2004) 242303.

[3] J. Adams *et al.* [STAR Collaboration], *"Forward neutral pion production in p+p and d+Au collisions at $\sqrt{s_N N} = 200~GeV$"*, arXiv:nucl-ex/0602011.

[4] D. E. Kharzeev, E. Levin, and L. McLerran, *Phys. Lett.* **B561** (2003) 93.

[5] J. Jalilian-Marian, Y. Nara and R. Venugopalan, *Phys. Lett.* **B577** (2003) 54.

[6] D. Kharzeev, Yu. V. Kovchegov, and K. Tuchin, *Phys. Rev.* **D66** (2003) 094013.

[7] R. Baier, A. Kovner and U. A. Wiedemann, Phys. Rev. D **68** (2003) 054009.

[8] J.L. Albacete, N. Armesto, A. Kovner, C.A. Salgado and U.A. Wiedemann, *Phys. Rev. Lett.* **92** (2004) 082001.

[9] J.P. Blaizot, F. Gelis, R. Venugopalan, Nucl. Phys. A **743** (2004) 13 ; *ibid.* (2004) 57.

[10] E. Iancu, K. Itakura, and D.N. Triantafyllopoulos, *Nucl. Phys.* **A742** (2004) 182.

[11] D. Kharzeev, Yu. V. Kovchegov, and K. Tuchin, *Phys. Lett.* **B599** (2004) 23.

[12] R. Baier, Y. Mehtar-Tani and D. Schiff, Nucl. Phys. **A764** (2006) 515.

[13] A. Dumitru, A. Hayashigaki, and J. Jalilian-Marian, *Nucl. Phys.* **A765** (2006) 464.

[14] A. Dumitru, A. Hayashigaki, and J. Jalilian-Marian, *Nucl. Phys.* **A770** (2006) 57.

[15] E. Iancu, K. Itakura and S. Munier, *Phys. Lett.* **B590** (2004) 199.

[16] L. McLerran and R. Venugopalan, *Phys. Rev.* **D49** (1994) 2233; *ibid.* **49** (1994) 3352; *ibid.* **50** (1994) 2225.

[17] E. Iancu, A. Leonidov and L. McLerran, *Nucl. Phys.* **A692** (2001) 583; *Phys. Lett.* **B510** (2001) 133; E. Ferreiro, E. Iancu, A. Leonidov, L. McLerran, *Nucl. Phys.* **A703** (2002) 489.

[18] E. Iancu, A. Leonidov and L. McLerran, *"The Colour Glass Condensate: An Introduction"*, arXiv:hep-ph/0202270. Published in *QCD Perspectives on Hot and Dense Matter*, Eds. J.-P. Blaizot and E. Iancu, NATO Science Series, Kluwer, 2002;
E. Iancu and R. Venugopalan, *"The Color Glass Condensate and High Energy Scattering in QCD"*, arXiv:hep-ph/0303204. Published in *Quark-Gluon Plasma 3*, Eds. R.C. Hwa and X.-N. Wang, World Scientific, 2003.

[19] I. Arsene *et al.* [BRAHMS Collaboration], *Nucl. Phys.* **A757** (2005) 1.

[20] A.M. Stasto, K. Golec-Biernat and J. Kwiecinski, Phys. Rev. Lett. **86** (2001) 596.

[21] E. Iancu, K. Itakura, and L. McLerran, *Nucl. Phys.* **A708** (2002) 327.

[22] A.H. Mueller and D.N. Triantafyllopoulos, *Nucl. Phys.* **B640** (2002) 331.

[23] D.N. Triantafyllopoulos, *Nucl. Phys.* **B648** (2003) 293.

[24] Yu. V. Kovchegov and A. H. Mueller, *Nucl. Phys.* **B529** (1998) 451.

[25] B.Z. Kopeliovich, A.V. Tarasov, and A. Schafer, *Phys. Rev.* **C59** (1999) 1609.

[26] A. Dumitru and L. McLerran, *Nucl. Phys.* **A700** (2002) 492.

[27] Yu. V. Kovchegov and K. Tuchin, *Phys. Rev.* **D65** (2002) 074026.

[28] A. Kovner and U. Wiedemann, *Phys. Rev.* **D64** (2001) 114002.

[29] C. Marquet, *Nucl. Phys.* **B705** (2005) 319.

[30] M. Braun, *Eur. Phys. J.* **C16** (2000) 337; *Phys. Lett.* **B483** (2000) 105.

[31] I. Balitsky, *Nucl. Phys.* **B463** (1996) 99; *Phys. Lett.* **B518** (2001) 235; hep-ph/0101042.

[32] J. Jalilian-Marian, A. Kovner, A. Leonidov and H. Weigert, *Nucl. Phys.* **B504** (1997) 415; *Phys. Rev.* **D59** (1999) 014014; J. Jalilian-Marian, A. Kovner, H. Weigert, *Phys. Rev.* **D59** (1999) 014015; A. Kovner, J. G. Milhano and H. Weigert, *Phys. Rev.* **D62** (2000) 114005.

[33] H. Weigert, *Nucl. Phys.* **A703** (2002) 823.

[34] Yu.V. Kovchegov, *Phys. Rev.* **D60** (1999), 034008; *ibid.* **D61** (1999), 074018.

[35] E. Iancu and A.H. Mueller, *Nucl. Phys.* **A730** (2004) 460; *Nucl. Phys.* **A730** (2004) 494.

[36] A.H. Mueller and A.I. Shoshi, *Nucl. Phys.* **B692** (2004) 175.

[37] E. Iancu, A.H. Mueller and S. Munier, *Phys. Lett.* **B606** (2005) 342.

[38] E. Iancu and D.N. Triantafyllopoulos, *Nucl. Phys.* **A756** (2005) 419; *Phys. Lett.* **B610** (2005) 253.

[39] A.H. Mueller, A.I. Shoshi, S.M.H. Wong, *Nucl. Phys.* **B715** (2005) 440.

[40] E. Levin, M. Lublinsky, *Nucl. Phys.* **A763** (2005) 172.

[41] A. Kovner, M. Lublinsky, *Phys. Rev.* **D71** (2005) 085004; *Phys. Rev. Lett.* **94** (2005) 181603.

[42] J.-P. Blaizot, E. Iancu, K. Itakura, D.N. Triantafyllopoulos, *Phys. Lett.* **B615** (2005) 221.

[43] Y. Hatta, E. Iancu, L. McLerran, A. Stasto, and D.N. Triantafyllopoulos, *Nucl. Phys.* **A764** (2006) 423, arXiv:hep-ph/0504182.

[44] I. Balitsky, *Phys. Rev.* **D72** (2005) 074027, arXiv:hep-ph/0507237.

[45] Y. Hatta, E. Iancu, C. Marquet, G. Soyez, D.N. Triantafyllopoulos, *"Diffusive scaling and the high–energy limit of deep inelastic scattering in QCD at large N_c"*, hep-ph/0601150.

[46] A.H. Mueller, *Nucl. Phys.* **B415** (1994) 373; A.H. Mueller, B. Patel, *Nucl. Phys.* **B425** (1994) 471; A.H. Mueller, *Nucl. Phys.* **B437** (1995) 107.

[47] G.P. Salam, *Nucl. Phys.* **B449** (1995) 589; *Nucl. Phys.* **B461** (1996) 512; A.H. Mueller, G.P. Salam, *Nucl. Phys.* **B475** (1996) 293.

[48] L.N. Lipatov, *Sov. J. Nucl. Phys.* **23** (1976) 338;
E.A. Kuraev, L.N. Lipatov and V.S. Fadin, *Zh. Eksp. Teor. Fiz* **72**, 3 (1977) (*Sov. Phys. JETP* **45** (1977) 199);
Ya.Ya. Balitsky and L.N. Lipatov, *Sov. J. Nucl. Phys.* **28** (1978) 822.

[49] S. Munier and R. Peschanski, *Phys. Rev. Lett.* **91** (2003) 232001; *Phys. Rev.* **D69** (2004) 034008; *ibid.* **D70** (2004) 077503.

[50] G. Soyez, *Phys. Rev.* **D72** (2005) 016007.

[51] R. Enberg, K. Golec–Biernat and S. Munier, *Phys. Rev.* **D72** (2005) 074021.

[52] For a recent review, see W. Van Saarloos, *Phys. Rep.* **386** (2003) 29.

[53] E. Brunet and B. Derrida, *Phys. Rev.* **E56** (1997) 2597; *Comp. Phys. Comm.* **121-122** (1999) 376; *J. Stat. Phys.* **103** (2001) 269.

[54] Yu.V. Kovchegov, *Phys. Rev.* **D72** 094009, arXiv:hep-ph/0508276.

[55] K. Golec-Biernat, L. Motyka, and A.M. Staśto, *Phys. Rev.* **D65** (2002) 074037.

[56] E. Levin and K. Tuchin, *Nucl. Phys.* **B573** (2000) 833; *Nucl. Phys.* **A691** (2001) 779; *Nucl. Phys.* **A693** (2001) 787.

[57] E. Levin and M. Lublinsky, *Phys. Lett.* **B521** (2001) 233; *Eur. Phys. J.* **C22** (2002) 647; M. Lublinsky, *Eur. Phys. J.* **C21** (2001) 513.

[58] K. Rummukainen and H. Weigert, *Nucl. Phys.* **A739** (2004) 183.

[59] C. Marquet, R. Peschanski and G. Soyez, *Nucl. Phys.* **A756** (2005) 399; C. Marquet and G. Soyez, *Nucl. Phys.* **A760** (2005) 208.

[60] L.V. Gribov, E.M. Levin, and M.G. Ryskin, *Phys. Rept.* **100** (1983) 1.

[61] C. Marquet, R. Peschanski and G. Soyez, *"Consequences of strong fluctuations on high-energy QCD evolution"*, hep-ph/0512186.

[62] E. Brunet, B. Derrida, A. H. Mueller and S. Munier, *"A phenomenological theory giving the full statistics of the position of fluctuating pulled fronts"*, arXiv:cond-mat/0512021.